Giant Tunability of Ferroelectric Polarization in $GdMn_2O_5$

N. Lee,[1] C. Vecchini,[2] Y. J. Choi,[1,3] L. C. Chapon,[4,5] A. Bombardi,[2] P. G. Radaelli,[6] and S-W. Cheong[1]

[1]*Rutgers Center for Emergent Materials and Department of Physics and Astronomy, Rutgers University, Piscataway, New Jersey 08854, USA*

[2]*Diamond Light Source Ltd., Harwell Science and Innovation Campus, Didcot, Oxfordshire OX11 0DE, United Kingdom*

[3]*Department of Physics and IPAP, Yonsei University, Seoul 120-749, Korea*

[4]*ISIS Facility, Rutherford Appleton Laboratory, STFC, Chilton, Didcot OX11 0QX, United Kingdom*

[5]*Institut Laue-Langevin, BP 156X, 38042 Grenoble, France*

[6]*Department of Physics, University of Oxford, Parks Road, Oxford OX1 3PU, United Kingdom*

(Received 6 December 2012; published 26 March 2013)

Giant tunability of ferroelectric polarization ($\Delta P = 5000\ \mu C/m^2$) in the multiferroic $GdMn_2O_5$ with external magnetic fields is discovered. The detailed magnetic model from x-ray magnetic scattering results indicates that the Gd-Mn symmetric exchange striction plays a major role in the tunable ferroelectricity of $GdMn_2O_5$, which is in distinction from other compounds of the same family. Thus, the highly isotropic nature of Gd spins plays a key role in the giant magnetoelectric coupling in $GdMn_2O_5$. This finding provides a new handle in achieving enhanced magnetoelectric functionality.

DOI: 10.1103/PhysRevLett.110.137203 PACS numbers: 75.85.+t, 75.25.−j, 77.22.Ej, 78.70.Ck

Multiferroics are fascinating materials where multiple orders out of ferroelectricity, ferroelasticity, and magnetism coexist and couple [1]. In particular, in magnetically driven ferroelectrics, the possibility of controlling the electric (magnetic) polarization by applying a magnetic (electric) field has attracted significant interest [2,3]. In these materials, the presence of competing interactions and/or magnetic frustration induces a magnetic order that breaks inversion symmetry, allowing ferroelectricity to develop. Both symmetric and antisymmetric parts of the magnetic exchange coupling can be coupled to the polar distortions. Antisymmetric exchange interaction is active in cycloidal magnetic multiferroics such as $LiCu_2O_2$ and $TbMnO_3$ [4–6] whereas multiferroicity in Ca_3CoMnO_6 [7] and $TbMn_2O_5$ [7–9] is primarily from symmetric exchange interactions. This latter mechanism can lead to large electric polarization (**P**) due to its nonrelativistic nature but compared with that of proper ferroelectrics such as $BaTiO_3$ ($P \sim 2 \times 10^5\ \mu C/m^2$) is still minuscule. For example, the polarization values of $LiCu_2O_2$, $TbMnO_3$, Ca_3CoMnO_6, and $TbMn_2O_5$ are 4, 800, 90, and 400 $\mu C/m^2$, respectively. Thus, one of the pressing challenges for magnetically driven multiferroics research is finding systems or means to enhance the magnitude of the polarization. In the conventional ferroelectrics $GdFeO_3$ and orthorhombic $HoMnO_3$ [10–12], the symmetric exchange interaction between rare-earth and transition-metal ions plays an essential role in producing large polarization ($\sim 1500\ \mu C/m^2$). The strong coupling between structural distortions and magnetic order can in principle lead to a large variation of the electric polarization under the application of magnetic fields. However, in known materials to date, the effect of strong magnetic fields is to either rotate tiny **P** by 90° in cycloidal multiferroics [13,14] or induce only a small variation of **P** ($\Delta P \sim 800\ \mu C/m^2$) in symmetric exchange striction compounds [9]. We discovered that $GdMn_2O_5$ exhibits an electrical polarization of unprecedented magnitude $P = 3600\ \mu C/m^2$ along the b axis. Furthermore, applying magnetic fields induces a giant change of P by $5000\ \mu C/m^2$, which is the largest among the known multiferroic systems.

The temperature dependence of **P** in zero magnetic field for two crystals (GMO1 and GMO2) is shown in Fig. 1(a). The onset of P_b for both crystals appears at $T_{N2} \sim 33$ K. In GMO2, the dielectric constant ε_b' starts to increase with a shoulder just below $T_{N1} \sim 40$ K and a sharp peak appearing near T_{N2}, consistent with the rapid growth of P_b. With decreasing temperature, P_b increases steadily until reaching a saturation value of $3600\ \mu C/m^2$ at 2 K. GMO1 shows a two-step-like increase of P_b below T_{N2} with smaller magnitude at 2 K and a broader anomaly in ε_b'. The second step of P_b at ~26 K may originate from pinned magnetoelectric domains with **P** opposite to the poling electric field. Figure 1(b) displays the magnetic field dependence of P_b measured at 2 K. Upon increasing H_a, P_b tends to decrease until it suddenly reverses at $H_a^{sf} \sim 4.7$ T, reaching $-2000\ \mu C/m^2$ in magnitude. Thus, the drastic change of P_b induced by the external magnetic field is on the order of $\Delta P_b \sim 5000\ \mu C/m^2$. Upon decreasing H_a from 9 T, P_b exhibits large magnetic hysteresis and does not recover the initial value at $H_a = 0$ T, possibly due to the creation of multiple magnetoelectric domains with opposite **P**. We also observed a repeatable flipping of P_b with H_a linearly changing between 0 and 5 T at 2 K [Fig. 1(c)]. The magnetic field of 5 T was chosen to minimize the magnetic hysteresis and maximize the variation of ferroelectric polarization during repetition.

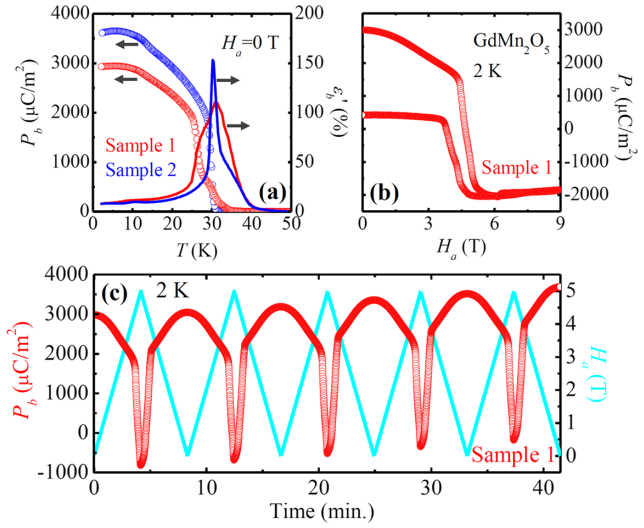

FIG. 1 (color online). (a) Temperature dependencies of electric polarizations and dielectric constants along the b axis under zero magnetic field for GMO1 (sample 1, in red) and GMO2 (sample 2, in blue). (b) H_a dependence of P_b at 2 K, where H_a was swept from 0 to 9 T, then back to 0 T after poling in $E_b \sim 10$ kV/cm and $H_a = 0$ T, for GMO1. (c) Repeated variation of P_b (red circles) at 2 K under the application of H_a (light blue lines) for GMO1. H_a was varied linearly between 0 and 5 T.

The sequential flipping of **P** continues without significant decay, and the abundant change of ferroelectric polarization induced by the magnetic field persists. The temperature and magnetic field dependencies of magnetization are shown in Figs. 2(a) and 2(b). The anomalies corresponding to $T = 33$ and 26 K are clearly shown in the temperature derivative of magnetization in the inset in Fig. 2(a). The isothermal M_a at 2 K displays spin-flop transitions around 5 T in accordance with the reversal of P_b.

In order to establish the magnetic structure responsible for this exceptional behavior, we performed x-ray magnetic scattering at the I16 Beamline (Diamond Light Source, UK) in off-resonance and at the Gd L_3-edge

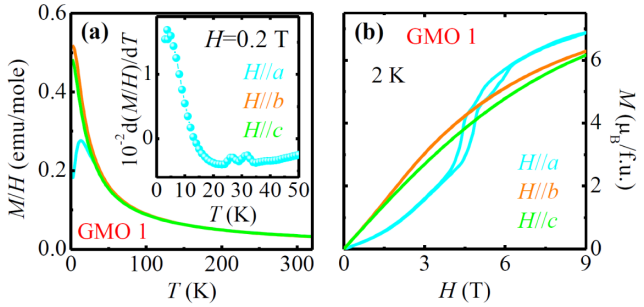

FIG. 2 (color online). (a) Temperature dependence of magnetization along the crystallographic axes for $H = 0.2$ T. Inset shows the temperature derivative of the susceptibility along the a axis. (b) Magnetic field dependence of magnetization along the three axes at 2 K.

(resonance) conditions. $GdMn_2O_5$ long range magnetically orders at T_{N1} with the incommensurate propagation vector $\mathbf{k}_{N1} \sim (0.49\,0\,0.18)$. This phase is stable down to T_{N2}, where $\mathbf{k}$ locks at the commensurate value $\mathbf{k}_{N1} = (1/2, 0, 0)$. In the commensurate (ferroelectric) phase in the vicinity of T_{N2}, the temperature dependence of the magnetic peaks intensities follows a Brillouin law $[\sim (1 - T/T_{N2})^{2\beta}]$ [Fig. 3(a)]. The critical exponents measured in nonresonant and resonant conditions are identical within the experimental error, respectively $\beta = 0.26 \pm 0.02$ and $\beta = 0.29 \pm 0.03$. This behavior indicates a unique order parameter with contribution from the Gd and Mn magnetization, in contrast to the observed induced magnetic ordering (secondary coupled order parameter) of Ho, Tb, and Er [15,16]. This different critical behavior and the stabilization of a magnetic phase

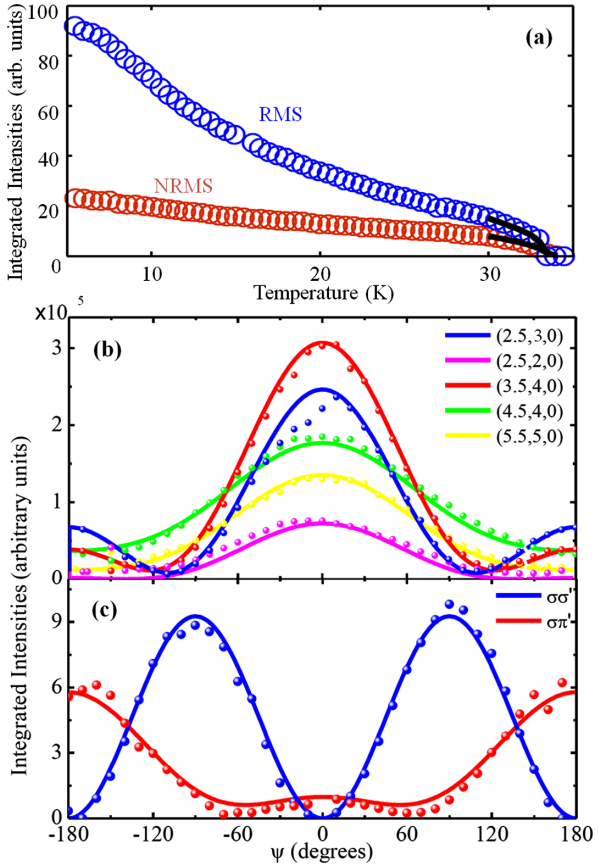

FIG. 3 (color online). (a) Temperature dependence of the (2.5 3 0) reflection in resonance (labelled RMS) and off resonance (labelled NRMS) multiplied by a factor of 10, collected at $\psi = 50$ and $\psi = 0$, respectively. The black lines are fits to the critical exponents. (b) Azimuthal dependence of the magnetic Bragg peaks intensities at 5 K at resonance. The azimuth value is given with respect to a reference in the (1 0 0) direction. The straight lines are fits to the data. (c) NRMS of the (2.5 3 0) reflection at 6.4 keV, in the $\sigma\sigma'$ (dark grey) and $\sigma\pi'$ (light grey) channels. The symbols containing the error bars show the experimental data points.

at a different symmetry point (X point) strongly suggests that the Gd ions, through Gd/Mn exchange, are actively driving the transition. Below $T \sim 30$ K, the slight difference in the slope between the temperature dependence of the resonant (RMS) and nonresonant magnetic scattering (NRMS) intensities [Fig. 3(a)] might be due to the presence of a small induced component on the not yet saturated Gd sites that cannot be disentangled. A model for the magnetic structure of the Gd sublattice has been derived from the azimuthal dependence of five magnetic reflections measured in resonant conditions at 5 K, shown in Fig. 3(a) [17]. The azimuthal scans present a twofold periodicity with maxima at positions close to $\psi = 0°$ and 180° indicating that the Gd moments are approximately aligned along the crystallographic a axis. The Gd magnetic configuration and the magnetic symmetry were found by a least-squares refinement of all azimuthal scans considered simultaneously. The full magnetic space group $P_a b 2_1 a$ ($P_a c a 2_1$ in conventional IT settings) corresponds to one (X_2) of the two irreducible representations allowed for the magnetic structure (X_1, X_2) and the order parameter in the special direction $(a, 0)$. Out of the six symmetry-allowed magnetic modes spanning X_1 and X_2, the proposed one is uniquely consistent with Gd moments in the ab plane and a ferroelectric axis along b. With this symmetry, only the moments on sites 1 and 2 [Fig. 4(a)], on one hand, and sites 3 and 4, on the other hand, are related by the twofold rotation, whereas the two sets are unrelated due to the loss of inversion symmetry. Finally, no changes in the energy dependence of the resonant signal or in the azimuthal scans were detected from data collected at $T = 5$, 15, 25, and 31 K using the (2.5 3 0) reflection, suggesting an unchanged Gd magnetic configuration with temperature. The complete magnetic structure, i.e., including the Mn magnetic ordering and the relative phase between Gd and Mn modulations, was probed using NRMS [17–19]. Under the assumption that $R\mathrm{Mn_2O_5}$ compounds share an almost identical magnetic configuration in each $\mathrm{Mn^{3+}/Mn^{4+}}$ layer, the Mn spins were fixed in the ab plane to that found for all the other commensurate structures of the series. By including the Gd contribution derived from the RMS work, the off-resonance data can be adequately fitted, as shown in Fig. 3(b). By supposing that the Mn ordered moments are saturated at the spin-expected value of $3\mu_B$ (octahedral site, $S = 3/2$) and $4\mu_B$ (pyramidal site, $S = 2$), one obtains an ordered moment for $\mathrm{Gd^{3+}}$ at 5 K of $\sim 5.14(4)\mu_B$ and $\sim 4.75(4)\mu_B$ for sites 1-2 and 3-4, respectively. Although the total magnetic structure factor is sensitive to the relative phase of the Mn moments with respect to the Gd moments, the NRMS $\sigma\pi$ data do not allow us to unequivocally distinguish between a ferromagnetic (FM) or antiferromagnetic (AFM) $\mathrm{Gd^{3+}}$-$\mathrm{Mn^{3+}}$ alignment. Preliminary neutron scattering on a recently grown isotopic $\mathrm{GdMn_2O_5}$ crystal confirms the latter arrangement [20]. Therefore, as reported in Fig. 4, the Gd moments are arranged almost antiparallel relative to the neighboring $\mathrm{Mn^{3+}}$ moments (pyramidal sites).

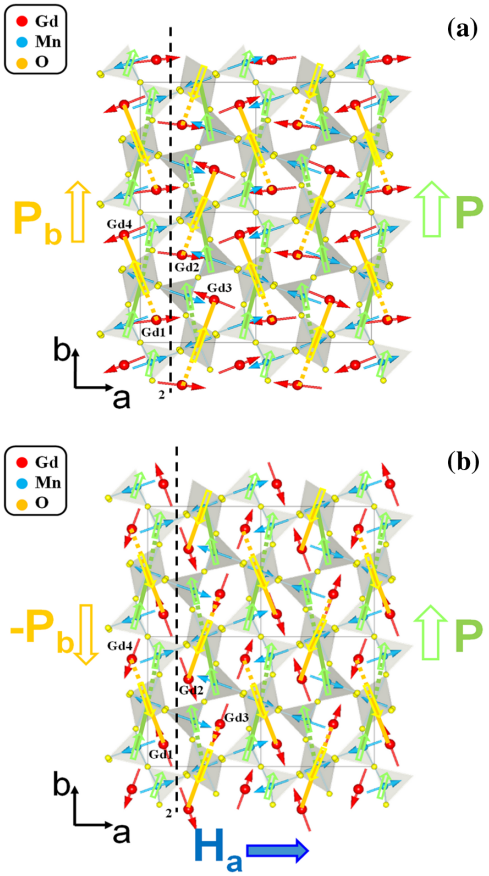

FIG. 4 (color online). (a) In-plane crystallographic and commensurate magnetic structure of $\mathrm{GdMn_2O_5}$ at 5 K. The solid and dotted lines indicate attractive and repulsive exchange interactions for Gd-Mn (yellow or light grey) and Mn-Mn (green or dark grey), respectively. Open (yellow or light grey and green or dark grey) arrows represent a schematics of the directions of the ionic displacements corresponding to the macroscopic polarization ($P + P_b$). The large (yellow or light grey) P_b and (green or dark grey) P arrows represent the polarization of the Gd and Mn magnetic sublattices, respectively. (b) In-plane spin structure showing the reversed direction of P_b (Gd polarization) under the application of H_a.

The magnetic structure stabilized below T_{N2} for $\mathrm{GdMn_2O_5}$ is the simplest of the series and yet supports ferroelectricity along b. Like other ferroelectric $R\mathrm{Mn_2O_5}$ in their most polar phase, k_x is locked at half, forming AFM chains along the a axis with constant moment amplitude. In contrast with other members, however, this is the only system for which $k_z = 0$, producing a FM stacking along c of the adjacent AFM planes. Two phenomena can explain such effect. First, eight-coordinated $\mathrm{Gd^{3+}}$ has a slightly larger ionic size (1.193 Å) than other rare earths (Tb = 1.18 Å, Dy = 1.16 Å, Ho = 1.15 Å, Er = 1.14 Å), which affects the $\mathrm{Mn^{4+}}$-$\mathrm{Mn^{4+}}$ direct exchange interaction through the Gd layer. Since longer

Mn-Mn interatomic distances promotes ferromagnetic direct exchange [21], the argument seems to hold for $GdMn_2O_5$ (Mn-Mn distance of 2.89 Å). Second, considering the relatively high transition temperatures where dipole interactions do not play a crucial role, it can be safely assumed that magnetism is very isotropic on the Gd site ($4f^7$ electronic configuration) and that the Gd moment direction will align along the spin direction of its strongest interacting neighbor. This is what is observed experimentally since the Gd moments are nearly collinear with first neighbor Mn^{3+} spins (Gd-Mn distance ~3.303 Å). The situation is very different in analogues with nonquenched orbital momentum displaying noncollinear arrangements of the R moments. Moreover, unlike any other ferroelectric RMn_2O_5, Gd has a large ordered moment in every layer due to the simple commensurate structure. This unique magnetic configuration has important consequences for the ferroelectric behavior. In fact, the symmetric exchange striction between Mn pairs cannot be uniquely responsible for the remarkable ferroelectricity in $GdMn_2O_5$. Note that a system such as YMn_2O_5 where the ferroelectricity results mainly from the Mn-Mn exchange striction displays a **P** of only 1000 $\mu C/m^2$, which is less than one third that found in $GdMn_2O_5$. Since the Gd spin configuration on its own breaks inversion symmetry, one expects a finite contribution to the polarization along b from the coupled polar ionic displacements allowed by symmetry (Γ_{4-} mode) on the Gd site and coordinated oxygens. Therefore, the magnetic structure of $GdMn_2O_5$ strongly indicates that the explanation for the additional source of **P** lies in the symmetric exchange striction mechanism of Gd-Mn spin pairs in the commensurate phase. In fact, the attraction between parallel Gd-Mn pairs gives the distortion producing the ferroelectricity along the b axis [yellow arrow in Fig. 4(a)] in the same direction of the ferroelectric **P** induced by Mn-Mn exchange striction. By comparison with $BiMn_2O_5$, in which the spin flop in the AFM chain under applied magnetic field is known to be responsible for the reversal of **P** [22], we speculate that upon applying H_a, Gd spins rotate by 90°, while the Mn moments, harder to pin, are likely to remain unchanged. This scenario switches the relative orientations of spin pairs (Gd-Mn and Mn-Mn) and therefore gives rise to the reversal of the ferroelectric polarization as shown in Fig. 4(b).

In summary, we have established that $GdMn_2O_5$ displays the largest ferroelectric polarization in zero magnetic field and the largest variation of polarization in a magnetic field among the magnetically driven ferroelectrics. Furthermore, the direction of the polarization can be repeatedly switched by an applied magnetic field. On the basis of the complete magnetic structure, we conclude that in addition to the Mn-Mn exchange striction mechanism, the Gd-Mn symmetric exchange striction is primarily responsible for the observed large ferroelectric polarization.

The work at Rutgers University was supported by DOE Grant No. DE-FG02-07ER46382.

[1] S.-W. Cheong and M. Mostovoy, Nat. Mater. **6**, 13 (2007).
[2] T. Kimura, T. Goto, H. Shintani, K. Ishizaka, T. Arima, and Y. Tokura, Nature (London) **426**, 55 (2003).
[3] P. G. Radaelli, L. C. Chapon, A. Daoud-Aladine, C. Vecchini, P. J. Brown, T. Chatterji, S. Park, and S.-W. Cheong, Phys. Rev. Lett. **101**, 067205 (2008).
[4] I. A. Sergienko, C. Şen, and E. Dagotto, Phys. Rev. Lett. **97**, 227204 (2006).
[5] S. Park, Y. J. Choi, C. L. Zhang, and S.-W. Cheong, Phys. Rev. Lett. **98**, 057601 (2007).
[6] S. Dong, R. Yu, S. Yunoki, J.-M. Liu, and E. Dagotto, Phys. Rev. B **78**, 155121 (2008).
[7] Y. J. Choi, H. T. Yi, S. Lee, Q. Huang, V. Kiryukhin, and S.-W. Cheong, Phys. Rev. Lett. **100**, 047601 (2008).
[8] L. C. Chapon, P. G. Radaelli, G. R. Blake, S. Park, and S.-W. Cheong, Phys. Rev. Lett. **96**, 097601 (2006).
[9] N. Hur, S. Park, P. A. Sharma, J. S. Ahn, S. Guha, and S.-W. Cheong, Nature (London) **429**, 392 (2004).
[10] N. Lee, Y. J. Choi, M. Ramazanoglu, W. Ratcliff, V. Kiryukhin, and S.-W. Cheong, Phys. Rev. B **84**, 020101 (2011).
[11] B. Lorenz, Y. Q. Wang, Y. Y. Sun, and C. W. Chu, Phys. Rev. B **70**, 212412 (2004).
[12] Y. Tokunaga, N. Furukawa, H. Sakai, Y. Taguchi, T.-h. Arima, and Y. Tokura, Nat. Mater. **8**, 558 (2009).
[13] T. Goto, T. Kimura, G. Lawes, A. P. Ramirez, and Y. Tokura, Phys. Rev. Lett. **92**, 257201 (2004).
[14] N. Aliouane, K. Schmalzl, D. Senff, A. Maljuk, K. Prokes, M. Braden, and D. N. Argyriou, Phys. Rev. Lett. **102**, 207205 (2009).
[15] G. Beutier, A. Bombardi, C. Vecchini, P. G. Radaelli, S. Park, S.-W. Cheong, and L. C. Chapon, Phys. Rev. B **77**, 172408 (2008).
[16] H. Kimura, S. Kobayashi, Y. Fukuda, T. Osawa, Y. Kamada, Y. Noda, I. Kagomiya, and K. Kohn, J. Phys. Soc. Jpn. **76**, 074706 (2007).
[17] M. Blume and D. Gibbs, Phys. Rev. B **37**, 1779 (1988).
[18] J. P. Hill and D. F. McMorrow, Acta Crystallogr. Sect. A **52**, 236 (1996).
[19] F. De Bergevin and M. Brunel, Acta Crystallogr., Sect. A: Found. Crystallogr. **37**, 314 (1981).
[20] C. Vecchini, L. C. Chapon, S.-W. Cheong, and P. G. Radaelli (to be published).
[21] In manganese metals, the crossover between AFM and FM is ~2.83 Å.
[22] J. W. Kim, S. Y. Haam, Y. S. Oh, S. Park, S.-W. Cheong, P. A. Sharma, M. Jaime, N. Harrison, J. H. Han, G.-S. Jeon, P. Coleman, and K. H. Kim, Proc. Natl. Acad. Sci. U.S.A. **106**, 15 573 (2009).